



# Impact of FDG-PET and Dynamic Contrast-Enhanced MRI in Comparison with DWI for N-Staging in Lung Cancer Patients

Paul Flechsig<sup>1,2,\*</sup>, Heike Zabeck<sup>3</sup>, Sebastian Reubold<sup>1</sup>, Christos Sachpekidis<sup>1,4</sup>, Hendrik Rathke<sup>1</sup>, Manuel Röhrich<sup>1</sup>, Tim Holland-Letz<sup>5</sup>, Claus-Peter Heussel<sup>6</sup>, Alexander Harms<sup>7</sup>, Hans-Ulrich Kauczor<sup>2,8</sup>, Uwe Haberkorn<sup>1,2,4</sup> and Frederik L. Giesel<sup>1,4,9</sup>

<sup>1</sup>Department of Nuclear Medicine, University Hospital Heidelberg, Heidelberg, Germany

<sup>2</sup>Translational Lung Research Center Heidelberg, German Center for Lung Research, Heidelberg, Germany

<sup>3</sup>Thorax Clinic at Heidelberg University, Division of Thoracic Surgery, Heidelberg, Germany

<sup>4</sup>Clinical Cooperation Unit, Department of Nuclear Medicine, German Cancer Research Center, Heidelberg, Germany

<sup>5</sup>Department of Biostatistics, German Cancer Research Center, Heidelberg, Germany

<sup>6</sup>Thorax Clinic at Heidelberg University, Division of Diagnostic and Interventional Radiology with Nuclear Medicine, Heidelberg, Germany

<sup>7</sup>Institute of Pathology, University Hospital Heidelberg, Heidelberg, Germany

<sup>8</sup>Diagnostic and Interventional Radiology Clinic, University Hospital Heidelberg, Heidelberg, Germany

<sup>9</sup>Department of Radiology, Columbia University Medical Center, New York, United States

\*Corresponding author: Department of Nuclear Medicine, University Hospital Heidelberg, INF 400, 69120, Heidelberg, Germany. Tel: +49-06221-56-38197, Fax: +49-06221-56-5473, Email: paul.flechsig@med.uni-heidelberg.de

Received 2018 March 13; Revised 2018 August 27; Accepted 2018 September 03.

## Abstract

**Background:** Regarding mediastinal N-staging in lung cancer patients, computed tomography (CT), magnetic resonance imaging (MRI), and integrated <sup>18</sup>Fluorine-fluorodeoxyglucose-positron emission tomography/CT (<sup>18</sup>F-FDG-PET/CT) are the most widespread imaging methodologies in clinical routine.

**Objectives:** In order to further extract information from non-invasive staging, we evaluated the use of <sup>18</sup>F-FDG-PET/CT and dynamic contrast enhanced (DCE) and diffusion-weighted imaging (DWI) MRI using histopathology as the diagnostic gold standard.

**Patients and Methods:** A total number of 50 patients had undergone MRI of the chest within two weeks prior to surgery for histopathological proof. DCE-MRI was evaluated on the basis of region of interest (ROI)-based signal intensity/time (SI/T) curves in the respective mediastinal lymph nodes (LNs). In total, 28 LNs could be allocated to the corresponding histopathological findings, as well as to corresponding findings in <sup>18</sup>F-FDG-PET/CT.

**Results:** Malignant LNs presented with significantly higher FDG uptake in PET. Significant differences between malignant and benign LNs were found for DCE-MRI regarding the parameters MaxE, 4-minutes value, SE, EP and EP/MaxE. In DWI-MRI, malignant LNs presented with significantly lower signal intensity compared to benign LNs ( $p < 0.01$ ). An apparent diffusion coefficient (ADC) threshold of 1528 mm<sup>2</sup>/s was found to exclude malignancy for LNs that are above the threshold.

**Conclusion:** <sup>18</sup>F-FDG-PET in addition with MRI that includes DWI might improve mediastinal N-staging, which is of interest in cases of FDG-equivocal LNs. An ADC threshold of 1528 mm<sup>2</sup>/s might potentially help to further classify LNs with indefinite PET-findings. DCE-MRI of mediastinal LNs seems not yet to be approved for clinical routine.

**Keywords:** Lung Cancer, staging, FDG-PET/CT, Magnetic Resonance Imaging, DWI

## 1. Background

In lung cancer patients, initial oncologic staging is usually performed using morphologic imaging such as computed tomography (CT), which is often complemented by functional imaging modalities, such as <sup>18</sup>Fluorine-fluorodeoxyglucose-positron emission tomography/computer tomography (<sup>18</sup>F-FDG-PET/CT) (1, 2), or in some cases also magnetic resonance imaging (MRI) (3). For therapeutic planning, loco-regional tumor growth, mediastinal lymph node (LN) infiltration and the absence

or presence of distant metastases is of vital importance to predict oncological outcome. Regarding nodal staging, the involvement of contralateral or multiregional mediastinal LNs often excludes patients from primary surgery (4, 5). False positive findings can occur in FDG-PET/CT due to inflammation in the lung and the associated mediastinal LNs (6). Therefore, histological confirmation of suspicious PET findings as part of invasive staging procedures is recommended by different guidelines (7), thus increasing the risk for potential side effects of invasive staging.

To extract further information from non-invasive  $^{18}\text{F}$ -FDG-PET/CT and MRI, metric and functional PET and MRI measures were evaluated, including diffusion and perfusion analyses as part of native and dynamic contrast-enhanced (DCE) MRI studies. In particular, the use of dynamic MR imaging with dedicated, contrast-enhanced MR protocols of the lung within a strategy adapted to the pulmonary circulation, has recently shown to be a simple and robust technique for the evaluation of lung lesions of different dignities (3). Moreover, in the setting of integrated PET/MRI, the combination of metabolic PET, as well as morphological and functional MR imaging using dedicated protocols for the evaluation of moving thoracic lung lesions and LNs, can potentially further improve nodal staging in patients with lung cancer. This is of interest, since recent studies evaluating the use of combined  $^{18}\text{F}$ -FDG-PET/MRI in most cases could not find significant advantages of the simultaneous use of PET and MRI in the staging of lung cancer patients (8-11).

## 2. Objectives

The hypothesis of this investigation was that possible malignant mediastinal LN involvement could be further characterized using diffusion-weighted imaging (DWI) and DCE MRI-sequences as part of a dedicated MR protocol for lung imaging.

## 3. Patients and Methods

### 3.1. Study Design and Patients

The study was conducted as a retrospective single-center analysis. From 2013 to 2016 a total number of 50 patients suffering from NSCLC was investigated with an MRI of the chest in our department, including diffusion- and DCE MR-imaging. All patients had additional  $^{18}\text{F}$ -FDG-PET/CT of the lung according to the clinical schedule. Imaging was performed within two weeks prior to surgery/histopathological sampling. The study was approved by the institutional review board and conducted according to the guidelines of the institutional review board (IRB) and within the bounds of good clinical practice according to the ethical principles that have their origin in the Declaration of Helsinki. Written informed consent was obtained from all patients.

### 3.2. $^{18}\text{F}$ -FDG-PET/CT

$^{18}\text{F}$ -FDG-PET/CT was performed as part of the clinical routine for reasons of preoperative staging reasons and therapeutic planning within two weeks prior to surgery including mediastinal LN-dissection. Patients with neoadjuvant radiation and/or chemotherapy were ruled out from the analysis. Patients were examined with a biograph 6

PET/CT scanner (Siemens Medical Solution, Knoxville, Tennessee, USA).

As recently described in the body of the literature (12, 13), after fasting for at least 8 hours,  $^{18}\text{F}$ -FDG-PET/CT was performed at a blood glucose level below 150 mg/dL, administering 4 Mega Becquerel / kilogram (MBq/kg) body weight of  $^{18}\text{F}$ -FDG intravenously. Quantitative PET evaluation was based on maximum standard uptake value (SUVmax) calculations 60 minutes after tracer injection. For reconstruction of CT images, the following reconstruction parameters were used: Slice thickness/reconstruction increment of 5.0/2.5 mm, standard soft-tissue reconstruction kernel B30.

### 3.3. MRI Technique

All MRI-studies in this research were performed with a dedicated protocol that is aligned with lung imaging as described in a recent publication by Koenigkam-Santos et al. (3). All MRI-measurements were performed using a 1.5-T MR scanner (Siemens Aera, Erlangen, Germany). Prior to the application of contrast agent (CA), morphological sequences were acquired as described in detail in the above mentioned study (3) using an identical protocol including T2-weighted pulse sequence images, half-fourier acquisition single turbo spin-echo (HASTE in coronal and transversal plane); T2-weighted BLADE sequences with fat suppression (FS) in the transversal plane; volumetric interpolated breath-hold examination (VIBE) images with and without FS in the transversal plane; dynamic free-breathing balanced steady-state free precession in the coronal plane, gradient echo images using overlapping slices ("cine effect"); and free breathing two-dimensional (2D) echo-planar diffusion-weighted imaging (DWI) with different b-values (0 - 800) in the transversal plane. For DCE-MRI, VIBE sequences with FS and constant sequence parameters were used. All sequences were acquired during consecutive breath holds with a slice thickness of 4 mm. After the application of CA, six acquisitions were acquired, including five in the axial view, and one in the coronal view (3rd minutes). Via the cubital vein, a single dose of a rapid bolus of 0.1 mmol Gadobutrol (Gadovist 1.0, Bayer Healthcare Pharmaceuticals, Leverkusen, Germany)/kg body weight was injected by intravenous administration. Therefore, an automatic power injector was used (2.5 mL/s). Initial flush was followed by 20 mL of 0.9% saline (same injection rate). A bolus detection technique (CARE bolus, 1 s time resolution) was used to adapt diagnostic acquisitions to the individual circulation time. Bolus detection was performed in the pulmonary trunk. Including the whole protocol, all examinations were performed within 20 - 25 minutes. During the whole study, no adverse events were observed.

### 3.4. Image Analysis

LN evaluations and post-processing including PET- and MRI-analysis were performed by an experienced radiologist (5 years) blinded to clinical information and to histological diagnosis. Findings in PET and MRI for each LN level were correlated with the histological gold standard as stated in the histopathological report taking the histological tumor subtype into account [adenocarcinoma (ADC), adenosquamous cell carcinoma (ADC-SQCC), neuroendocrine tumors (carcinoid), squamous cell carcinoma (SQCC), non-small cell lung cancer not otherwise specified (NSCLC NOS)]. Histopathological analyses were based on surgical resection including mediastinal LN-dissection within two weeks after PET- and MR-imaging.

MRI-analyses were performed as described in detail by Koenigkam-Santos et al. (3) quantifying the following parameters: relative signal intensity (SI%), time point of arrival of CA after injection ( $t_{CA}$ ), type of SI-time curves for each LN, time of early peak of contrast enhancement (EP), slope of contrast enhancement (SE), maximum of contrast enhancement in all acquisitions (MaxE), relation of EP to MaxE, washout ratio (WOR), relative enhancement 4 minutes after CA injection (4 minutes) (3). As proposed in many studies before, shapes of curves were classified into four different types (3, 14) as follows: curve type A (fast, intense early increase of SI, subsequent fast and significant decrease [washout]); curve type B (fast, intense early increase of SI, lacking washout); curve type C (mild / moderate progressive increase of SI in all acquisitions); curve type D (no significant increase of SI over non-enhanced level). Detailed definition of the parameters EP, SE and WOR were described previously (3).

### 3.5. Statistical Analysis

For statistical analysis, SigmaPlot (Systat Software GmbH, Erkrath) and R version (The R Foundation for Statistical Computing, Vienna, Austria) were used. Median and quantile values for signal intensity in MRI, Bq/mL and SUVmax in PET with 95% confidence interval were calculated and illustrated in Box-and-Whisker plots or as multiple lines with error-bars in a scatter chart. In order to take possible correlations between lesions on the same patient into account, applied statistical tests were undertaken using likelihood ratio tests in a linear mixed model, with "patient id" as a random factor. All graphical displays refer to individual lesions. Differences were considered significant at  $P < 0.05$  in a likelihood ratio (LR) test.

## 4. Results

### 4.1. Histological Findings and Patient Population

Due to the strict selection criteria, a total number of 28 LNs could clearly be correlated in DWI-MRI, DCE-MRI,  $^{18}F$ -

FDG-PET/CT and histopathology [12 patients (9 male, median age: 63 years)]. The other patients had to be excluded for reasons of outdated or external  $^{18}F$ -FDG-PET/CT with missing cross-calibration, due to missing histopathological proof out of one of the examined mediastinal LNs due to systemic tumor spread or biopsies out of a distant metastasis, or due to unclear or missing assignment between histopathological findings, and the corresponding findings in MRI and/or  $^{18}F$ -FDG-PET/CT. Among the 28 LNs, tissue samplings were performed via mediastinal LN dissections as part of surgical resections in all patients with histopathology as diagnostic gold standard (Figures 1 and 2). Out of the 28 LNs, 20 LNs in 11 patients were of benign histology; 8 LNs in 4 patients were malignant and out of them 3 had also histologically proven benign LNs. Out of the 12 patients who were analyzed, tumor entities were as follows: ADC (n = 4), ADC-SQCC (n = 2), carcinoid, (n = 3), SQCC (n = 1), NSCLC NOS (n = 2). The 8 malignant LNs included the following tumor entities: ADC (n = 5), ADC-SQCC (n = 1), carcinoid, (n = 2).

### 4.2. PET Imaging

Regarding PET-acquisition 60 minutes after FDG-administration, malignant LNs presented with significantly higher SUVmax-values (mean  $4.71 \pm 2.89$ ) compared to benign LNs (mean  $1.85 \pm 0.57$ ,  $P = 0.02$ , Figures 1 - 3) and mediastinal blood pool (mean  $2.02 \pm 0.42$ ,  $P < 0.01$ , Figures 1 - 3).

### 4.3. MR-Imaging with DCE-Analysis and DWI

SI-time curves could be created for all of the 28 LNs, and derived perfusion parameters were calculated. Regarding benign LNs, 19 out of 20 LNs presented with curve type A (Figure 4A and B) (Table 1), one out of 20 LNs presented with curve type B. Regarding malignant LNs, five out of eight LNs presented with curve type B, three out of eight LNs presented with curve type C (Figure 4A and B) (Table 1). None of the examined LNs presented with curve type D.

In comparison to benign LNs, malignant LNs demonstrated lower values for EP ( $P = 0.03$ ) and SE ( $P < 0.01$ , Table 1). In contrast, malignant LNs presented with higher values with respect to the parameter MaxE ( $P < 0.01$ ) and 4 minutes ( $P < 0.01$ ) (Table 1).

Following the above mentioned results, the curve type A is associated with benign LN findings, and the curve types B and C seem to represent malignant LN infiltration.

Regarding ADC analysis, malignant lesions presented with significantly lower values (mean  $1318.6 \text{ mm}^2/\text{s} \pm 125.7$ ) compared to benign LNs (mean  $1645.5 \text{ mm}^2/\text{s} \pm 304.7$ ) (Figure 5) ( $P < 0.01$ ). A possible cut-off value for the exclusion of malignancy in suspicious LNs was found for a signal intensity of  $1528 \text{ mm}^2/\text{s}$ , since 100% of all LNs above the  $1528 \text{ mm}^2/\text{s}$  cut-off were benign, while 53% of all lesions below

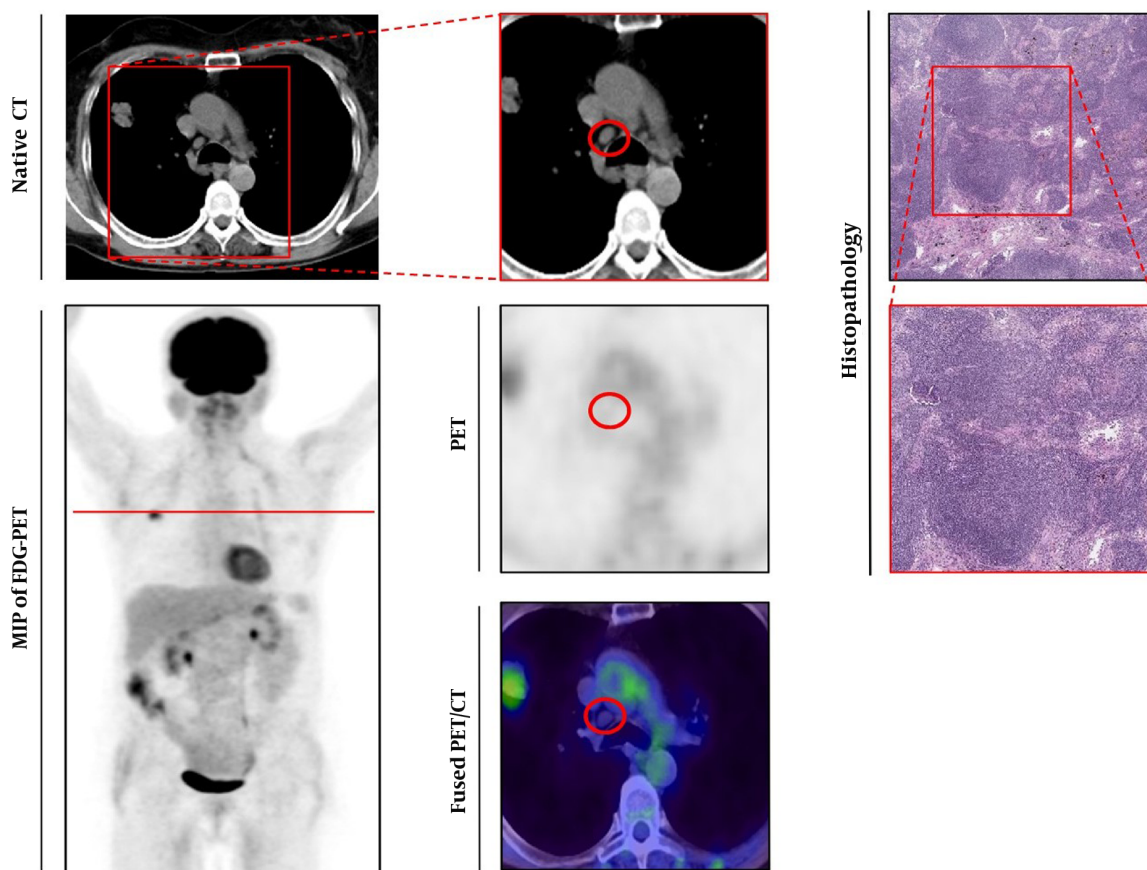


**Figure 1.** Histologically-proven benign lymph node. Left series demonstrates axial view of native CT (upper line) and maximum intensity projection (MIP) of  $^{18}\text{F}$ -fluorodeoxyglucose-positron emission tomography ( $^{18}\text{F}$ -FDG-PET) below. Middle series with magnified native CT (upper line), PET (below), and fused  $^{18}\text{F}$ -FDG-PET/CT-image (lower line). Right series demonstrates histopathological gold standard of benign lymph node (LN) (Haematoxylin and Eosin (H & E) staining, upper line 40-times magnified). The observed LN is indicated by a red circle, red line in the MIP of FDG-PET/CT indicated section plane for axial slices.

the  $1528 \text{ mm}^2/\text{s}$  limit were malignant (sensitivity: 1.0, specificity: 0.65; positive predictive value: 0.53; negative predictive value: 1.0, overall accuracy: 0.75) (Figure 5). This might potentially help to exclude malignancy from suspicious LNs above the proposed signal intensity.

Respective receiver operating characteristic (ROC)-curves and area under the curve (AUC)-values for the PET-parameter SUVmax, as well as for the MRI-parameters ADC, EP, SE, MaxE, EP/MaxE and 4 minutes are mentioned in Figure 6.

## 5. Discussion

In order to differentiate between benign and malignant mediastinal LNs, we found significant differences in the aspects of FDG uptake in  $^{18}\text{F}$ -FDG-PET/CT, as well as in DWI- and DCE-MRI analysis within the identical patient population, thus confirming the hypothesis of this study.

Nevertheless, some of the findings need critical discussion, since prior studies focusing on DCE-MRI, DWI-MRI and DCE-CT of mediastinal LNs detected a huge variability of findings that are contradictory in some aspects. Regarding ADC analysis in this study, it was possible to suggest an ADC-based cut-off value of  $1528 \text{ mm}^2/\text{s}$  in order to exclude malignancy from LNs that are above the threshold of  $1528 \text{ mm}^2/\text{s}$ . This might be of interest, especially in a pre-operative setting, in cases of FDG-equivocal findings, since dedicated DWI sequences can easily be introduced into routine MR protocols and also in the setting of integrated PET/MRI.

Regarding the use of FDG-PET/CT examinations, we found a significantly higher FDG uptake in malignant LNs in the static scan 60 minutes after glucose injection, which is already well known as part of the daily clinical routine (6, 12, 13). As recently described by Sauter et al. there were some inverse correlations between the vascular aspect of tumor supply measured by CT perfusion and the glucose

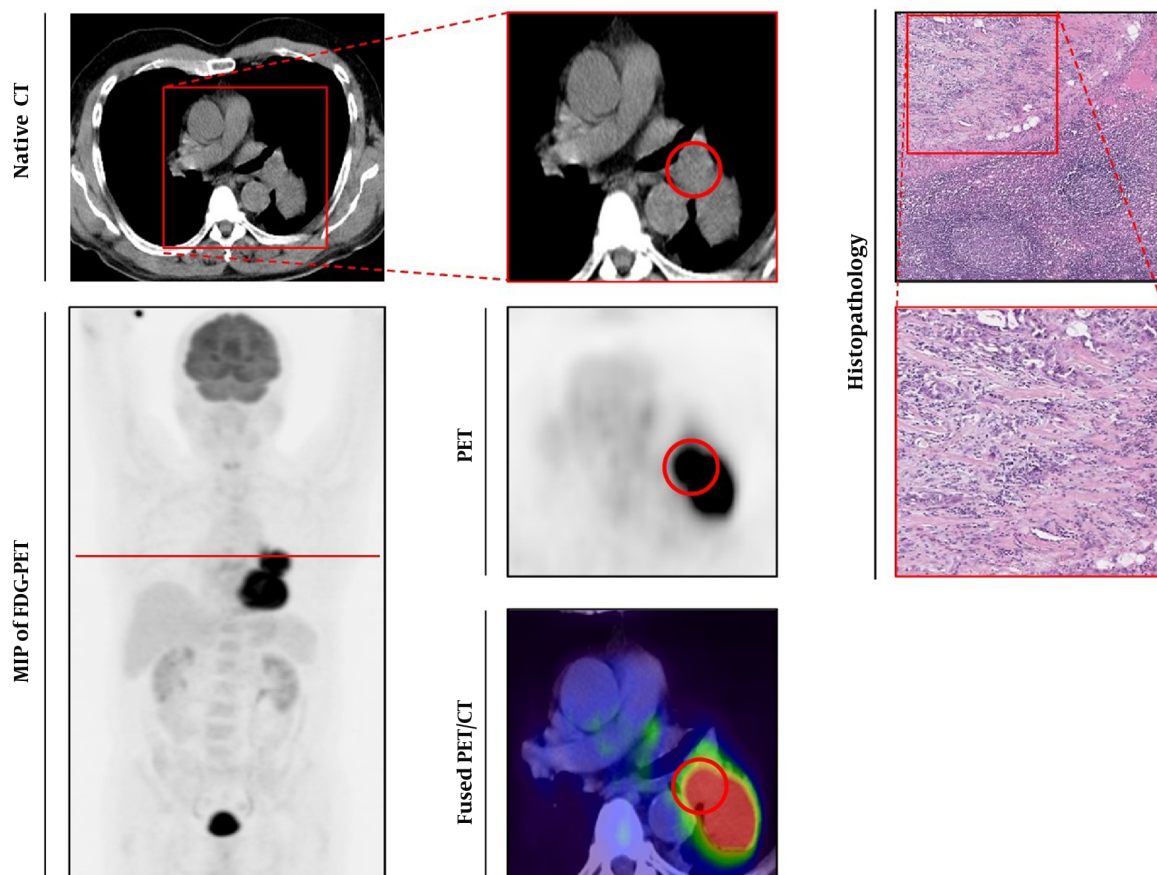


**Figure 2.** Histologically-proven malignant lymph node. Left series demonstrates axial view of native CT (upper line) and maximum intensity projection (MIP) of  $^{18}$ Fluorine-fluorodeoxyglucose-positron emission tomography ( $^{18}$ F-FDG-PET) below. Middle series with magnified native CT (upper line), PET (below), and fused  $^{18}$ F-FDG-PET/CT-image (lower line). Right series demonstrates histopathological gold standard of malignant lymph node (LN) (Haematoxylin and Eosin (H & E) staining, upper line 40-times magnified). The observed LN is indicated by a red circle, red line in the MIP of FDG-PET/CT indicated section plane for axial slices.

dependent tumor metabolism measured by PET studies when evaluating mediastinal LNs in NSCLC patients. In contrast to findings in mediastinal LNs, Sauter et al. discovered that perfusion and glucose metabolism were uncoupled when examining the primary tumor (15). This is of interest, since the present study found conflicting results in some aspects when comparing the derived perfusion parameters from the present LN analysis with prior results derived from the analyses of the primary tumors or solitary pulmonary nodules. In this context, data derived from DCE-MRI of the observed LNs demonstrated significantly higher values for MaxE and the 4- minutes value for malignant LNs, while malignant lesions presented with significantly lower values for the parameters SE, EP and EP/MaxE. These findings correlate with the presence of type B and type C curves in malignant LNs, while benign LNs demonstrated an overabundance of type A curves. These findings

are contrary to previous findings from Koenigkam-Santos et al. (3) and Schaefer et al. (14), where curve types A and B were associated with malignancy, while the curve types C and D were in most cases common in benign findings when examining solitary pulmonary nodules instead of mediastinal LNs. In particular, findings concerning the parameters SE, EP and EP/MaxE are opposing findings that were derived by Koenigkam-Santos, who examined the perfusion of primary tumors using the same MR protocol (3), and to findings published by Ohno et al. who introduced initial experiments with DCE MRI of solitary pulmonary nodules (16). As stated in a previous study (3), different findings of measured perfusion parameters can be partly explained by the different techniques that were used for DCE measurements in the different perfusion studies used in the past (14, 16-22). Nevertheless, the robustness of the applied MR protocol in the present study for the evalua-

**Table 1.** Lymph Node Characteristics in DCE MRI<sup>a</sup>

	Diagnosis		P value
	Benign	Malignant	
<b>N lesions</b>	20	8	
<b>MRI size, mm</b>	0.93 (0.7 - 1.1)	0.81 (0.7 - 1.0)	0.12
<b>Curve type, N</b>			
A	19	0	
B	1	5	
C	0	3	
D	0	0	
<b>EP, SI%</b>	4.1 (0 - 16.3)	1.7 (1.1 - 1.6)	0.03
<b>SE, SI%/s</b>	1.37 (0.13 - 2.50)	0.37 (0.18 - 0.84)	< 0.01
<b>MaxE, SI%</b>	49.1 (3 - 98)	124 (72 - 296)	< 0.01
<b>EP/MaxE, %</b>	1.0 (1.0 - 1.0)	0.72 (0.58 - 0.84)	< 0.01
<b>WOR, %</b>	81.4 (38 - 98)	n.m	n.m
<b>4 min, %</b>	7.85 (< 0 - 55)	124 (72 - 296)	< 0.01

Abbreviations: EP, early peak of contrast enhancement; DCE, dynamic contrast enhanced; MaxE, maximum of contrast enhancement in all acquisitions; n.m, not measurable; SE, slope of contrast enhancement; WOR, washout ratio; SI, signal intensity.

<sup>a</sup>Derived parameters from DCE-MRI of benign and malignant lymph nodes (LNs). All values are mean values with minimum and maximum values in parentheses, with corresponding P values above.

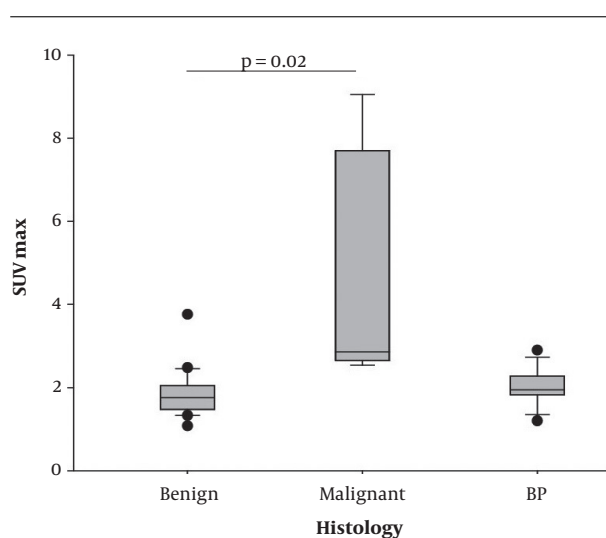


**Figure 3.** Positron emission tomography (PET)-analysis. Box plots of maximum standard uptake value (SUVmax) calculated by static PET images 60 minutes after fluorodeoxyglucose (FDG) injection. Significantly higher SUVmax in malignant lymph nodes (LNs) compared to benign LNs ( $P = 0.02$ ), BP, blood pool.

tion of small lesions  $\geq 8$  mm has already been noted by Koenigkam-Santos et al. which is a necessary condition for the evaluation of suspicious LNs (3). Moreover, the protocol is adjusted to patients suffering from lung diseases since only five breath holds are necessary during the 4 min of DCE imaging. In addition, a study published by Spira et al. focusing on CT perfusion analysis of LNs in patients with lung cancer found no significant differences in perfusion characteristics between benign and malignant LNs (23). Taking all the above-mentioned data from prior studies into account, the technique of DCE measurement in LN-staging for patients with lung cancer is not yet reliably applicable in a daily clinical setting.

Regarding ADC-based analysis of the DWI studies, significantly lower signal intensity was found in malignant LNs compared to benign LNs. These findings correlate with prior results from Schaarschmidt et al. and Ye et al. who were both examining ADC signal in LN-metastases of patients with lung cancer (24, 25). Lower ADC signal in metastatic LNs are also found in a study published by Liang et al., who examined ADC signal intensity in LNs of patients suffering from head and neck cancer (26), substantiating the general nature of lower ADC signal in LN-metastases with an increased cellularity as compared to benign LNs. Moreover, an ADC cut-off of  $1528 \text{ mm}^2/\text{s}$  could be proposed to exclude malignancy from LNs that are above the aforementioned threshold, which can potentially be valuable in clinical routine, not only when applied simultaneously in an integrated PET/MRI setting, but also as an additive se-

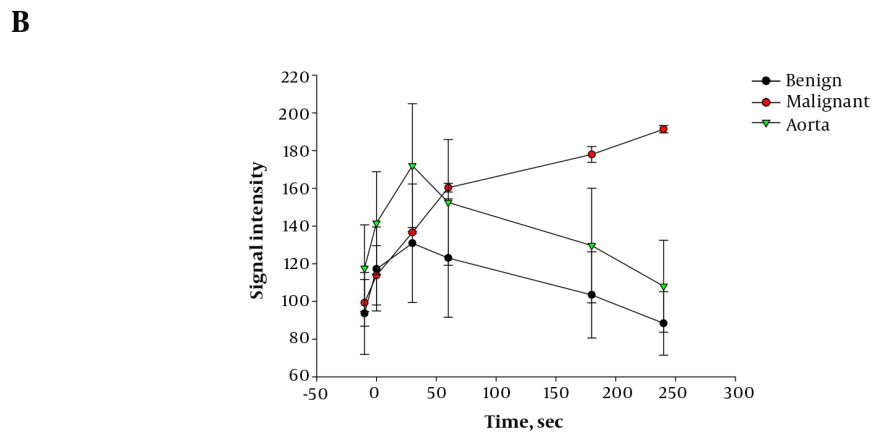
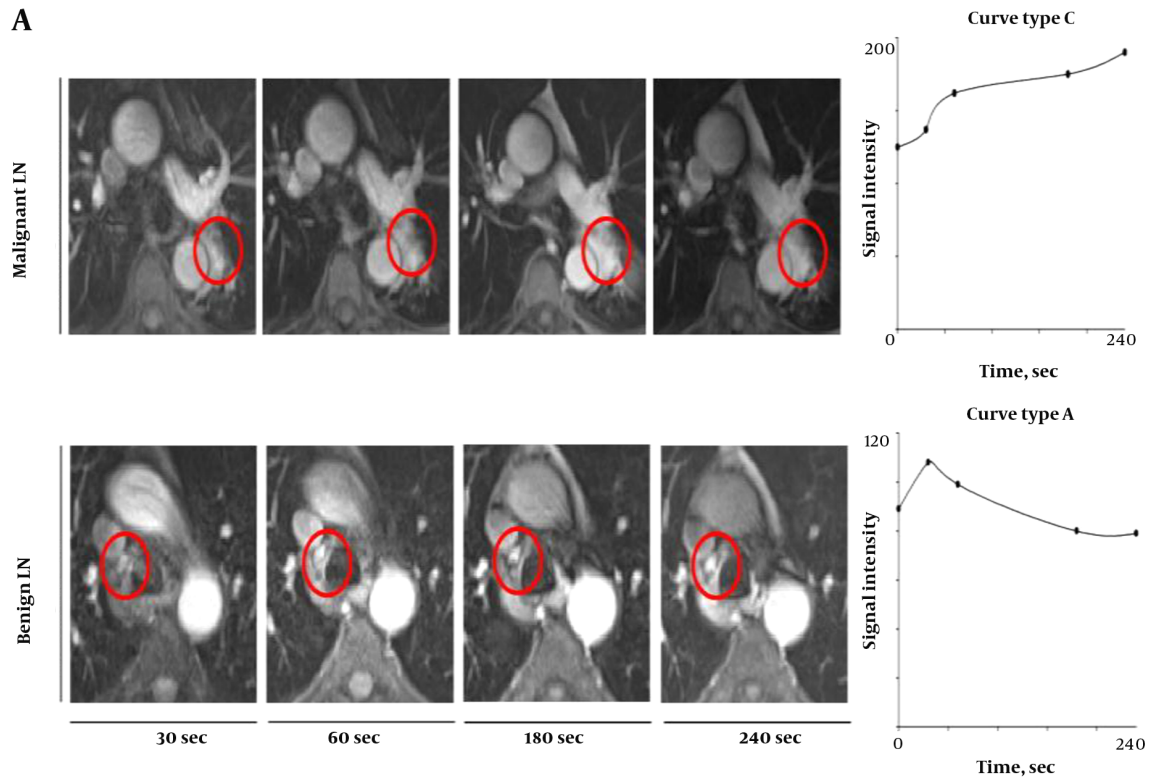


**Figure 4.** Dynamic contrast enhanced (DCE)-MRI. A, DCE-MRI of lymph nodes (LNs), axial view of dynamic contrast-enhanced LNs, 30, 60, 180 and 240 seconds after injection of contrast agent (CA). Upper line demonstrates above mentioned malignant LN, lower line demonstrates above mentioned benign LN. Right series with correlating perfusion curve of LN. B, Signal intensity over time in DCE-MRI, plot of signal intensity during DCE measurement in benign LNs (black line) and malignant LNs (red line). Green line indicates signal intensity in aorta.

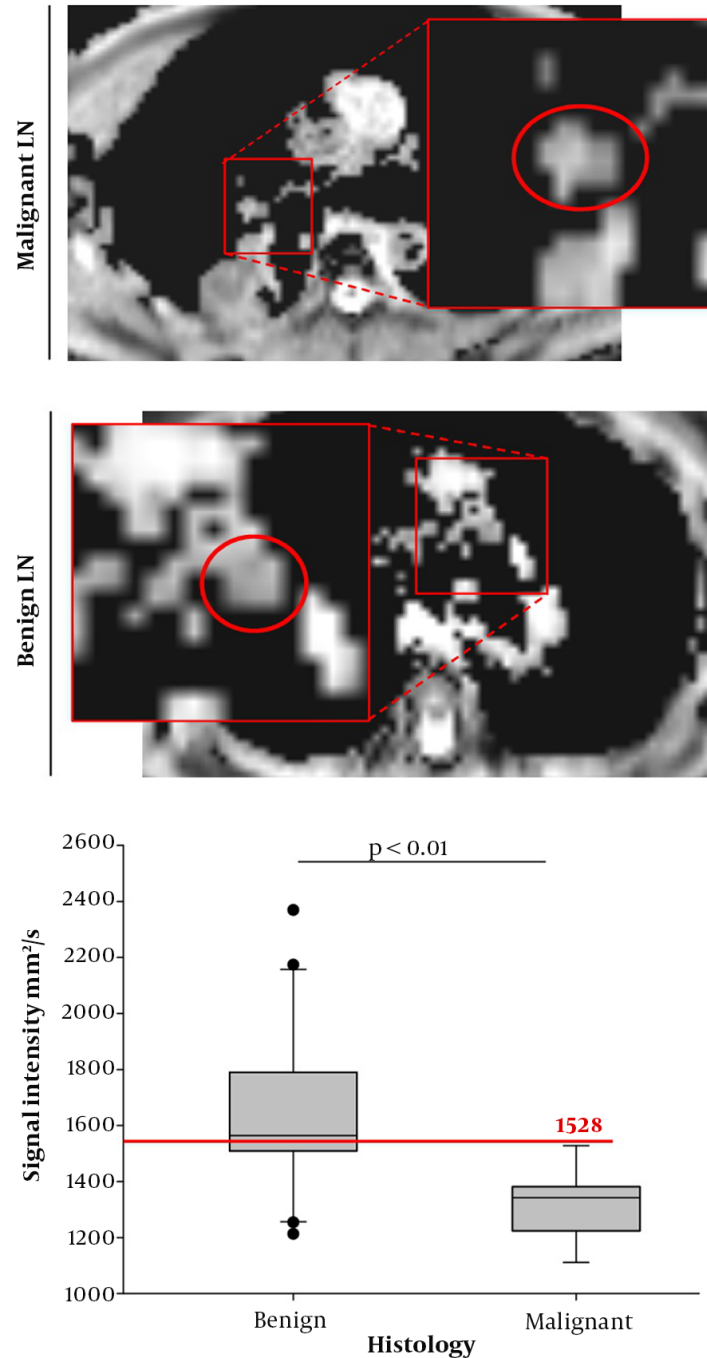


**Figure 5.** MRI with diffusion weighted imaging (DWI): Apparent diffusion coefficient (ADC) of malignant and benign lymph nodes (LNs). Left series demonstrates exemplarily chosen malignant LN (upper line) and exemplarily chosen lower LN (lower line). Right series shows Box Plot of ADC measurements with the derived threshold of 1528 in order to exclude malignancy (red line).

quential MR study to further classify LNs with equivocal findings in integrated <sup>18</sup>F-FDG-PET/CT.

The present study has limitations, especially due to the

relatively low number of histologically-proven LNs with consecutive PET and MRI findings within a period of two weeks prior to surgery. In order to increase the number of

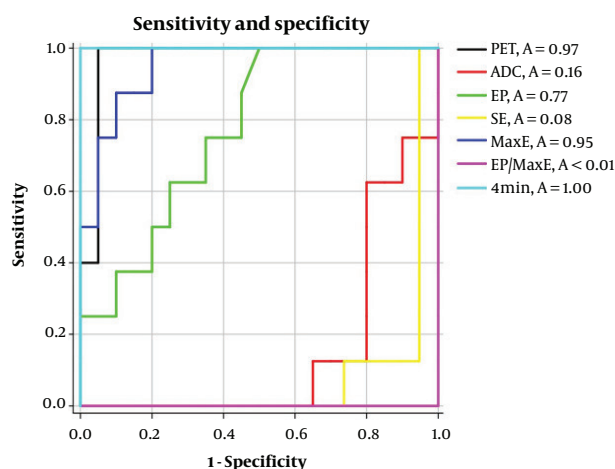


**Figure 6.** Sensitivities and specificities for all applied parameters. Area under the curve (AUC) for the positron emission tomography (PET)-parameter maximum standard uptake value (SUVmax) (black line), and the measured MRI parameters including apparent diffusion coefficient (ADC) (red line), early peak of contrast enhancement (EP) (green line), slope of contrast enhancement (SE) (yellow line), maximum of contrast enhancement in all acquisitions (MaxE) (dark blue line), EP/MaxE (purple line) and 4 minutes (light blue line).

lesions and patients participating in the study, a prospective multicenter setting could potentially be of interest for future trials.

Furthermore, it is mandatory to check robustness of introduced findings against changes of MRI- and PET/CT-scanners, and findings should be re-evaluated in more heterogeneous patient populations, best performed in prospective multi-center-trials. The use of the dedicated MR protocol applied in the present study with sequential use of PET and MRI needs further validation within integrated PET/MRI examinations; moreover, its impact on pre-operative tumor/node/metastasis (TNM) staging should be further evaluated, which could potentially improve the relatively poor results that have been published in previous PET/MRI studies regarding the aspect of clinical impact of integrated PET/MRI on TNM-staging in lung cancer patients (8-11, 27).

In conclusion, DWI MRI of mediastinal LNs in the context of sequential PET- and MRI-examinations or in the setting of integrated PET/MRI seems to be promising for non-invasive N-staging in lung cancer patients, especially when using the proposed threshold of  $1528 \text{ mm}^2/\text{s}$ . This is clinically relevant in cases of equivocal PET findings, and can potentially help to guide later invasive LN sampling to high yield targets. Dynamic contrast-enhanced MRI needs further scientific evaluation before its integration into clinical routine.

## Footnotes

**Authors' Contributions:** Study concept and design, Paul Flechsig, Frederik L. Giesel, Claus-Peter Heussel, Hans-Ulrich Kauczor, Sebastian Reubold and Heike Zabeck; analysis and interpretation of data, Paul Flechsig, Frederik L. Giesel, Sebastian Reubold, Alexander Harms and Christos Sachpekidis; drafting of the manuscript, Christos Sachpekidis, Paul Flechsig, Uwe Haberkorn, Frederik L. Giesel, Manuel Röhrich, Hendrik Rathke, Tim Holland-Letz and Claus-Peter Heussel; critical revision of the manuscript for important intellectual content, Paul Flechsig, Heike Zabeck, Sebastian Reubold, Christos Sachpekidis, Hendrik Rathke, Manuel Röhrich, Frederik L. Giesel, Alexander Harms, Hans-Ulrich Kauczor, Uwe Haberkorn and Frederik L. Giesel; statistical analysis, Paul Flechsig and Tim Holland-Letz

**Conflict of Interests:** There is no potential conflict of interests that is relevant to this article.

**Ethical Considerations:** The study was approved by the institutional review board and conducted according to the guidelines of the IRB and within the bounds of good clinical practice according to the ethical principles that have their origin in the Declaration of Helsinki. Written informed consent was obtained from all patients.

**Financial Disclosure:** None declared.

**Funding/Support:** None declared.

## References

- Kratochwil C, Haberkorn U, Giesel FL. [PET/CT for diagnostics and therapy stratification of lung cancer]. *Radiologe*. 2010;**50**(8):684-91. German. doi: [10.1007/s00117-009-1960-6](https://doi.org/10.1007/s00117-009-1960-6). [PubMed: [20652216](https://pubmed.ncbi.nlm.nih.gov/20652216/)].
- Abramyuk A, Appold S, Zophel K, Hietschold V, Baumann M, Abolmaali N. Quantitative modifications of TNM staging, clinical staging and therapeutic intent by FDG-PET/CT in patients with non small cell lung cancer scheduled for radiotherapy—a retrospective study. *Lung Cancer*. 2012;**78**(2):148-52. doi: [10.1016/j.lungcan.2012.08.001](https://doi.org/10.1016/j.lungcan.2012.08.001). [PubMed: [22922126](https://pubmed.ncbi.nlm.nih.gov/22922126/)].
- Koenigkam-Santos M, Optazait E, Sommer G, Safi S, Heussel CP, Kauczor HU, et al. Contrast-enhanced magnetic resonance imaging of pulmonary lesions: Description of a technique aiming clinical practice. *Eur J Radiol*. 2015;**84**(1):185-92. doi: [10.1016/j.ejrad.2014.10.007](https://doi.org/10.1016/j.ejrad.2014.10.007). [PubMed: [25455411](https://pubmed.ncbi.nlm.nih.gov/25455411/)].
- Tournoy KG, Keller SM, Annema JT. Mediastinal staging of lung cancer: novel concepts. *Lancet Oncol*. 2012;**13**(5):e221-9. doi: [10.1016/S1470-2045\(11\)70407-7](https://doi.org/10.1016/S1470-2045(11)70407-7). [PubMed: [22554550](https://pubmed.ncbi.nlm.nih.gov/22554550/)].
- Rami-Porta R, Call S. Invasive staging of mediastinal lymph nodes: Mediastinoscopy and remediastinoscopy. *Thorac Surg Clin*. 2012;**22**(2):177-89. doi: [10.1016/j.thorsurg.2011.12.003](https://doi.org/10.1016/j.thorsurg.2011.12.003). [PubMed: [22520285](https://pubmed.ncbi.nlm.nih.gov/22520285/)].
- Flechsig P, Kratochwil C, Schwartz LH, Rath D, Moltz J, Antoch G, et al. Quantitative volumetric CT-histogram analysis in N-staging of 18F-FDG-equivocal patients with lung cancer. *J Nucl Med*. 2014;**55**(4):559-64. doi: [10.2967/jnumed.113.128504](https://doi.org/10.2967/jnumed.113.128504). [PubMed: [24525209](https://pubmed.ncbi.nlm.nih.gov/24525209/)].
- Goekenjan G, Sitter H, Thomas M, Branscheid D, Flentje M, Griesinger F, et al. [Prevention, diagnosis, therapy, and follow-up of lung cancer. Interdisciplinary guideline of the German Respiratory Society and the German Cancer Society—abridged version]. *Pneumologie*. 2011;**65**(8):e51-75. German. doi: [10.1055/s-0030-1256562](https://doi.org/10.1055/s-0030-1256562). [PubMed: [21830177](https://pubmed.ncbi.nlm.nih.gov/21830177/)].

8. Schaarschmidt BM, Grueneisen J, Metzenmacher M, Gomez B, Gauler T, Roesel C, et al. Thoracic staging with (18)F-FDG PET/MR in non-small cell lung cancer - does it change therapeutic decisions in comparison to (18)F-FDG PET/CT? *Eur Radiol.* 2017;**27**(2):681-8. doi: [10.1007/s00330-016-4397-0](https://doi.org/10.1007/s00330-016-4397-0). [PubMed: 27180186].
9. Lee SM, Goo JM, Park CM, Yoon SH, Paeng JC, Cheon GJ, et al. Preoperative staging of non-small cell lung cancer: Prospective comparison of PET/MR and PET/CT. *Eur Radiol.* 2016;**26**(11):3850-7. doi: [10.1007/s00330-016-4255-0](https://doi.org/10.1007/s00330-016-4255-0). [PubMed: 26883332].
10. Heusch P, Buchbender C, Kohler J, Nensa F, Gauler T, Gomez B, et al. Thoracic staging in lung cancer: Prospective comparison of 18F-FDG PET/MR imaging and 18F-FDG PET/CT. *J Nucl Med.* 2014;**55**(3):373-8. doi: [10.2967/jnumed.113.129825](https://doi.org/10.2967/jnumed.113.129825). [PubMed: 24504054].
11. Huellner MW, de Galiza Barbosa F, Husmann L, Pietsch CM, Mader CE, Burger IA, et al. TNM staging of non-small cell lung cancer: Comparison of PET/MR and PET/CT. *J Nucl Med.* 2016;**57**(1):21-6. doi: [10.2967/jnumed.115.162040](https://doi.org/10.2967/jnumed.115.162040). [PubMed: 26471696].
12. Giesel FL, Schneider F, Kratochwil C, Rath D, Moltz J, Holland-Letz T, et al. Correlation between SUVmax and CT radiomic analysis using lymph node density in PET/CT-based lymph node staging. *J Nucl Med.* 2017;**58**(2):282-7. doi: [10.2967/jnumed.116.179648](https://doi.org/10.2967/jnumed.116.179648). [PubMed: 27660141].
13. Flechsigs P, Frank P, Kratochwil C, Antoch G, Rath D, Moltz J, et al. Radiomic analysis using density threshold for FDG-PET/CT-based n-staging in lung cancer patients. *Mol Imaging Biol.* 2017;**19**(2):315-22. doi: [10.1007/s11307-016-0996-z](https://doi.org/10.1007/s11307-016-0996-z). [PubMed: 27539308].
14. Schaefer JF, Vollmar J, Schick F, Vonthein R, Seemann MD, Aebert H, et al. Solitary pulmonary nodules: Dynamic contrast-enhanced MR imaging-perfusion differences in malignant and benign lesions. *Radiology.* 2004;**232**(2):544-53. doi: [10.1148/radiol.2322030515](https://doi.org/10.1148/radiol.2322030515). [PubMed: 15215548].
15. Sauter AW, Spira D, Schulze M, Pfannenbergs C, Hetzel J, Reimold M, et al. Correlation between [(1)(8)F]FDG PET/CT and volume perfusion CT in primary tumours and mediastinal lymph nodes of non-small-cell lung cancer. *Eur J Nucl Med Mol Imaging.* 2013;**40**(5):677-84. doi: [10.1007/s00259-012-2318-2](https://doi.org/10.1007/s00259-012-2318-2). [PubMed: 23306806].
16. Ohno Y, Hatabu H, Takenaka D, Adachi S, Kono M, Sugimura K. Solitary pulmonary nodules: Potential role of dynamic MR imaging in management initial experience. *Radiology.* 2002;**224**(2):503-11. doi: [10.1148/radiol.2242010992](https://doi.org/10.1148/radiol.2242010992). [PubMed: 12147849].
17. Pauls S, Mottaghy FM, Schmidt SA, Kruger S, Moller P, Brambs HJ, et al. Evaluation of lung tumor perfusion by dynamic contrast-enhanced MRI. *Magn Reson Imaging.* 2008;**26**(10):1334-41. doi: [10.1016/j.mri.2008.04.005](https://doi.org/10.1016/j.mri.2008.04.005). [PubMed: 18538522].
18. Zou Y, Zhang M, Wang Q, Shang D, Wang L, Yu G. Quantitative investigation of solitary pulmonary nodules: Dynamic contrast-enhanced MRI and histopathologic analysis. *AJR Am J Roentgenol.* 2008;**191**(1):252-9. doi: [10.2214/AJR.07.2284](https://doi.org/10.2214/AJR.07.2284). [PubMed: 18562755].
19. Chang YC, Yu CJ, Chen CM, Hu FC, Hsu HH, Tseng WY, et al. Dynamic contrast-enhanced MRI in advanced nonsmall-cell lung cancer patients treated with first-line bevacizumab, gemcitabine, and cisplatin. *J Magn Reson Imaging.* 2012;**36**(2):387-96. doi: [10.1002/jmri.23660](https://doi.org/10.1002/jmri.23660). [PubMed: 22517425].
20. Kono R, Fujimoto K, Terasaki H, Muller NL, Kato S, Sadohara J, et al. Dynamic MRI of solitary pulmonary nodules: Comparison of enhancement patterns of malignant and benign small peripheral lung lesions. *AJR Am J Roentgenol.* 2007;**188**(1):26-36. doi: [10.2214/AJR.05.1446](https://doi.org/10.2214/AJR.05.1446). [PubMed: 17179342].
21. Mamata H, Tokuda J, Gill RR, Padera RF, Lenkinski RE, Sugarbaker DJ, et al. Clinical application of pharmacokinetic analysis as a biomarker of solitary pulmonary nodules: Dynamic contrast-enhanced MR imaging. *Magn Reson Med.* 2012;**68**(5):1614-22. doi: [10.1002/mrm.24150](https://doi.org/10.1002/mrm.24150). [PubMed: 22231729]. [PubMed Central: PMC3335927].
22. Schaefer WM, Kaiser HJ, Kuehl H, Koch KC, Nowak B, Buell U. Quantification of left ventricular volumes and ejection fraction from 16- and rebinned 8-frame gated 99mTc-tetrofosmin SPECT. Comparison of 4D-MSPECT and QGS. *Nuklearmedizin.* 2007;**46**(1):22-8. doi: [10.1055/s-0037-1616622](https://doi.org/10.1055/s-0037-1616622). [PubMed: 17299651].
23. Spira D, Wecker M, Spira SM, Hetzel J, Spengler W, Sauter A, et al. Does volume perfusion computed tomography enable differentiation of metastatic and non-metastatic mediastinal lymph nodes in lung cancer patients? A feasibility study. *Cancer Imaging.* 2013;**13**(3):323-31. doi: [10.1102/j1470-7330.2013.0033](https://doi.org/10.1102/j1470-7330.2013.0033). [PubMed: 23876521]. [PubMed Central: PMC3719054].
24. Ye X, Chen S, Tian Y, You B, Zhang W, Zhao Y, et al. A preliminary exploration of the intravoxel incoherent motion applied in the preoperative evaluation of mediastinal lymph node metastasis of lung cancer. *J Thorac Dis.* 2017;**9**(4):1073-80. doi: [10.21037/jtd.2017.03.110](https://doi.org/10.21037/jtd.2017.03.110). [PubMed: 28523162]. [PubMed Central: PMC5418274].
25. Schaarschmidt BM, Buchbender C, Nensa F, Grueneisen J, Gomez B, Kohler J, et al. Correlation of the apparent diffusion coefficient (ADC) with the standardized uptake value (SUV) in lymph node metastases of non-small cell lung cancer (NSCLC) patients using hybrid 18F-FDG PET/MRI. *PLoS One.* 2015;**10**(1). e0116277. doi: [10.1371/journal.pone.0116277](https://doi.org/10.1371/journal.pone.0116277). [PubMed: 25574968]. [PubMed Central: PMC4289066].
26. Liang L, Luo X, Lian Z, Chen W, Zhang B, Dong Y, et al. Lymph node metastasis in head and neck squamous carcinoma: Efficacy of intravoxel incoherent motion magnetic resonance imaging for the differential diagnosis. *Eur J Radiol.* 2017;**90**:159-65. doi: [10.1016/j.ejrad.2017.02.039](https://doi.org/10.1016/j.ejrad.2017.02.039). [PubMed: 28583628].
27. Fraioli F, Screaton NJ, Janes SM, Win T, Menezes L, Kayani I, et al. Non-small-cell lung cancer resectability: Diagnostic value of PET/MR. *Eur J Nucl Med Mol Imaging.* 2015;**42**(1):49-55. doi: [10.1007/s00259-014-2873-9](https://doi.org/10.1007/s00259-014-2873-9). [PubMed: 25120040]. [PubMed Central: PMC4244545].